mathematics

MDPI

Article

Targeting Monoamine Oxidase B for the Treatment of Alzheimer's and Parkinson's Diseases Using Novel Inhibitors Identified Using an Integrated Approach of Machine Learning and Computer-Aided Drug Design

Arif Jamal Siddiqui [1,*], Sadaf Jahan [2], Maqsood Ahmed Siddiqui [3], Andleeb Khan [4], Mohammed Merae Alshahrani [5], Riadh Badraoui [1] and Mohd Adnan [1]

[1] Department of Biology, College of Science, University of Ha'il, Ha'il P.O. Box 2440, Saudi Arabia
[2] Department of Medical Laboratory Sciences, College of Applied Medical Sciences, Majmaah University, Al Majmaah 11952, Saudi Arabia
[3] Department of Zoology, College of Science, King Saud University, P.O. Box 2455, Riyadh 11451, Saudi Arabia
[4] Department of Pharmacology and Toxicology, College of Pharmacy, Jazan University, Jazan 45142, Saudi Arabia
[5] Department of Clinical Laboratory Sciences, Faculty of Applied Medical Sciences, Najran University, 1988, Najran 61441, Saudi Arabia
* Correspondence: ar.siddiqui@uoh.edu.sa; Tel.: +966-557399031

Abstract: Neurological disorders are disorders characterized by progressive loss of neurons leading to disability. Neurotransmitters such as nor-adrenaline, dopamine, and serotonin are partially regulated by the enzyme monoamine oxidase (MAO). Treatments for conditions like Alzheimer's, Parkinson's, anxiety, and depression involve the use of MAOIs. To target MAO enzyme inhibition, various scaffolds are prepared and evaluated, including modified coumarins, chromone carboxylic acid substituents, pyridazine derivatives, and indolylmethylamine. The research presented here focuses on combining different computational tools to find new inhibitors of the MAO-B protein. We discovered 5 possible chemical inhibitors using the above computational techniques. We found five molecular inhibitors with high binding affinity using computational methods. These five molecules showed a high binding affinity; they are −10.917, −10.154, −10.223, −10.858, and −9.629 Kcal/mol, respectively. Additionally, the selected inhibitors were further examined by in vitro activity, and their binding affinity was confirmed using an enzyme-based assay. In summary, the computational studies performed here using molecular dynamics and free energy calculations can also be used to design and predict highly potent derivatives as MAO-B inhibitors, and these top inhibitors help in the development of novel drugs for neurological diseases such as Alzheimer's and Parkinson's.

Keywords: CADD; computer biology; Alzheimer's; dynamics; pharmacophore; free energy calculation; docking

MSC: 92-08

Citation: Siddiqui, A.J.; Jahan, S.; Siddiqui, M.A.; Khan, A.; Alshahrani, M.M.; Badraoui, R.; Adnan, M. Targeting Monoamine Oxidase B for the Treatment of Alzheimer's and Parkinson's Diseases Using Novel Inhibitors Identified Using an Integrated Approach of Machine Learning and Computer-Aided Drug Design. *Mathematics* **2023**, *11*, 1464. https://doi.org/10.3390/math11061464

Academic Editor: Ricardo Lopez-Ruiz

Received: 22 January 2023
Revised: 21 February 2023
Accepted: 15 March 2023
Published: 17 March 2023

1. Introduction

Biogenic amines and neurotransmitters are oxidatively deaminated by the mitochondrial enzyme monoamine oxidase (MAO) [1]. This flavoenzyme is responsible for the oxidative deamination of hormones, neurotransmitters, and dietary amines. MAO's primary role is to block neurotransmitter amines from acting in the brain and other peripheral tissues. It also protects the brain from several amines, including tyramine, phenylethylamine, and benzylamine [2]. For synaptic neurotransmission to function properly, dopamine (DA), norepinephrine (NE), and the monoamine serotonin (5-HT) must be broken down by the MAO in the brain [3]. Its role has been summarized in Figure S1. The enzyme is mainly

found in the blood platelets and the brain. MAO resides in glial cells, and its level decreases with neuronal cell death [4]. So enzyme levels naturally increase with age because neuronal cell death increases with age. Additionally, its increases have been shown to promote cell degeneration by generating hydrogen peroxides, which iron then converts into extremely deadly oxygen free radicals, causing cell death [5,6]. The primary symptomatic treatment of Parkinson's disease is with MAO-B inhibitors [7,8]. However, the use of MAO-B drugs to treat Alzheimer's disease has been justified by the age-related increase in MAO-B enzyme activity and the neuroprotective role of MAO-B inhibitors [6]. Some well-known inhibitors are selegiline [9], safinamide [10], and rasagiline [11]. Older MAOIs, including iproniazid, are non-selective and irreversible. They also had a wide range of side effects and dietary restrictions as they could cause the cheese reaction, a severe hypertensive crisis when consumed with foods high in tyramine [12].

Previous studies showed that the structure-based design of inhibitors targets MAO-B protein [13,14]. On the other hand, in a separate study, authors have shown that xanthone-containing core rings also indicate a very good binding affinity for development as an MAO-B inhibitor [13]. In some studies, coumarin-based scaffolds have been optimized to design novel inhibitors for the MAO-B protein using the QSAR approach [14–16]. Also, the isoxazole derivatives have been substituted at the para position of the phenyl ring and have been developed as a new scaffold to inhibit MAO-B protein [17]. Recently, phytochemicals from Ocimum basilicum have been used to treat Parkinson's disease because of their therapeutic potential against MAO-B [18]. However, we could not find any studies that used both machine learning and other computational studies to identify inhibitors from the ZINC database, which encouraged us to undertake this work.

The crystal structure of this inhibitor with its receptor MAO-B, along with other known inhibitors at the binding site (Table S1), provided valuable structural insight into how the different ligands bind to the MAO-B binding site. The main objective of our studies was identifying putative inhibitors for the enzyme using ML and other computational approaches that open a new arena for the design of novel potent inhibitors against the enzyme. The methodology we have used in our studies has been summarized in Figure 1.

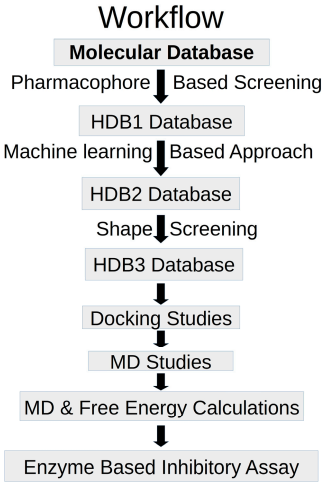

Figure 1. Workflow employed for identifying the potent ligands against MAO-B protein using various computational approaches.

2. Materials and Methods

2.1. Binding Pocket Analysis

The characterization of the binding site for the MAO-B protein was carried out using Schrödinger's SiteMap module [19]. SiteMap tool uses protein structure to identify binding pockets, their size, functionality, and the extent of their solvent exposure. The high-resolution crystal structure 2XFN was used for structural studies [20]. Chimera-1.16 [21]

was used for molecular interaction studies, and Gromac's version 20.0.7 [22] was used for time-dependent stability studies for the protein-ligand structure of MAO B [23].

2.2. Protein and Ligand Preparation

The Protein Data Bank provided the MAO-B crystal structure using the crystal structure 2XFN [24]. The Protein Preparation Wizard module of the Maestro software was used to prepare the structure. The receptor has been dehydrated, hydrogen atoms have been added, and the structure has been energy minimized to minimize constraints and poor contacts. Finally, the protein structure was reduced using the OPLS4 force field [25]. Two different databases, namely ZINC and MayBridge, were downloaded and saved in structure data format. The libraries were downloaded in July 2022, with more than 20 million compounds in aggregate. The ligands were prepared to determine a correct 3D structure using the LigPrep module [26]. In addition, the ligand conformation was optimized using the OPLS4 force field.

2.3. Pharmacophore-Based Approach

A pharmacophore-based virtual screen of the ZINC database was used to identify potential leads. The ZINC database includes more than 2 million compounds. First, the databases were extracted and prepared for the virtual screening process with the phase module [27]. The primary screening was performed using the pharmacophore model using the PHASE module. This module can be used for hit identification, lead optimization, and core hopping using the spatial arrangement of ligand or structure binding pocket or both. The retrieved hits were another measure of ADME properties by Schrödinger-2022.1's QikProp module [28,29]. The hits were then organized based on their predicted biological activities, adaptive values, and drug-like properties. After the structures of the various compounds were established, a minimum energy conformational model was calculated for the molecules using the default settings. Hydrophobic substructures, positively ionizable H-bond donor, H-bond acceptor, and ring aromaticity features were used to create pharmacophore models. Various pharmacophoric models with common features have been formulated for MaO-B inhibitors. Various scaffolds previously described as starting point structures for the development of molecules as MAO-B inhibitors were overlapped to generate a pharmacophore hypothesis showing a 4- or 5-feature model.

2.4. ML-Based Approach Screening

The dataset on the molecular activity of MAO-B protein inhibitors was extracted from the ChEMBL database [24]. In total, 5093 molecules were having reported activities against the MAO-B molecules. Molecules with reported IC50 values for the receptor were downloaded, and the data were processed. The data was divided into binary classes of active and inactive datasets to model binary classification models using machine learning. Descriptors were calculated for the molecules with activity as well as for decoys using the PaDEL package [25]. We calculated the MACCS, Pubchem, and GraphOnly descriptors for the datasets. The descriptor data was then used for training purposes. Numerous published studies point to applications of machine learning (ML) in the drug discovery pipeline [26–28]. We used the scikit-learn ML module to create models [29]. Scikit learn is a software package containing various algorithms to classify data using python. These algorithms are called estimators. Every estimator can be used to fit data using 2 inputs, namely samples matrix (x) and target values (y). The size of x is represented as rows and columns, while y is usually a 1d array. It has many built-in packages for building regression and classification models. We have used numerous algorithms to classify our data. The separation of the data into training and test datasets was done using a ratio of 75:25 for training and testing samples, as this ratio achieved good top model accuracy. For the 70:30 ratio, we noted a slight decrease in training accuracy, which prompted us to use the 75:25 ratio. Since there are numerous binary classification algorithms available, we have used the top models that are most commonly used to solve classification problems in

drug discovery. These include Support Vector Machine Model (SVM), Logistic Regression (LR), XGBoost (XGB), Decision Tree (DT), Multi-Layered Perceptron (MLP), and Random Forest [30–35]. SVM uses supervised learning models for classifying data. This algorithm finds a hyperplane in the N dimension to classify data points distinctly. Logistic regression uses logistic function to model dependent variables. In summary, this algorithm computes the sum of input features and calculates the logistic of the final result. XGB uses a gradient boosting framework to classify the different problems efficiently. This algorithm minimizes an objective function that combines a convex loss function and penalty term for model complexity. The training proceeds iteratively to decrease residual errors to make the final prediction. The decision tree algorithm uses simple learning decision rules based on data features to classify data. This method approximates the target function producing discrete values by using inductive inference. The process starts from the root node and classifies the corresponding feature attribute and its corresponding value until we reach the leaf node. MLP algorithm iteratively trains the model by updating the partial derivatives loss function with respect to the parameters of the model. Generally, this algorithm has 3 layers which includes one hidden layer. Cross-validation methods are used to find ideal values for optimizing the values. Weight adjustment training is performed by using backpropagation. Random forest classifies a large number of decision trees as an ensemble. Each tree in a random forest spits out a class prediction, and the class having the most votes is the final model. Settings used for these algorithms in previous reports were used in our current methodology to predict inhibitors [36–45]. Also, the mathematical equations of these algorithms have been elaborated in previous reports [46–51]. The various ML models were evaluated using several statistical values. We measured variables, such as accuracy, precision, recall, and receiver operating characteristic (ROC) curves, to evaluate the different ML models. Models with top scores in the training and test sets were selected for screening the ZINC database.

2.5. Shape-Based Screening Approach

One or more files, a phase database, or a shape query can be tested using the Shape Screening application [52]. The shape screening method helps screen molecules from databases having similar spatial constraints. The query is targeted differently to each conformer of a given molecule, and similarity was calculated using overlapping hard sphere volumes. Both single and multiple templates can serve as a form query. Here we have used both single and groups of template structures by overlapping the available crystal structures (Table S1). MacroModel atom typing was used for shape screening (imposes the most stringent conditions for matching) [53]. Each molecule produced 100 conformers while retaining up to 10 different conformations.

2.6. Docking-Based Approach

In this score-based screen, shortlisted hits were docked against MAO-B by ML- and the pharmacophore-based approach. The Schrödinger 2022.1 [54,55] Glide module was used for docking studies. Glide is a highly cited docking approach that uses conformation, orientation, and positional space to identify ligand poses. Using the receptor grid generation, a grid box of ($20 \times 20 \times 20$) was calculated to represent the shape and properties of the receptor. The Schrödinger suite's LigPrep and ConfGen tools were then used to generate a stable ligand conformation. Docking of the co-crystallized ligand to the protein binding site helped optimization of the docking parameters. As a result, test substances are then docked in the specified lattice box. The van der Waals scaling value was set to 1.0 while the partial atomic charge limit was set to 0.25 and the Coulomb VdW limit to 50 kcal/mol to reduce the potential for the non-polar part of the protein. In addition, the previously prepared protein was used in the docking assay, which explored the different binding interactions of the hits. The scoring function calculates the ranking of energy-minimized poses.

2.7. MD Studies of Protein-Ligand Complex

The stability of predicted protein-ligand complexes in the molecular dynamics simulations (MD) studies were performed using the gromacs 20.0.7 package [23]. Gromacs is a highly cited software that can decipher time-dependent protein motion. Numerous studies have been published examining the applicability of MD studies to determine protein–ligand stability [56–60]. Solvation was performed in a cubic box model using TIP3P water molecules with 12 radii as the boundary. The protein had a net negative charge, neutralized by adding an equal number of sodium ions by replacing water molecules. The system was relaxed for 100,000 steps using the steepest decent energy minimization. The energy minimization was achieved by the overall convergence criterion (Em) set to 10.0 KJ/mol. Isothermal-isochoric equilibration and isotropic pressure were performed using PME (Particle Mesh Ewald) scheme and Parrinello-Rahman scheme for 200,000 steps each. Finally, the system was made to run for 200 nanoseconds for MD studies.

2.8. Enzyme-Based Inhibitory Assay

To validate our methodology for identifying new compounds using the calculation protocol, we performed an enzyme-based assay using the MAO-B assay kit. Kit catalog number M7441 was a 96-well microplate assay kit. The reaction was performed using an Amplex Red Assay Kit. The positive control was prepared by adding an equal volume of buffer solution instead of a sample solution. Blank samples were prepared by adding an equal volume of buffer solution instead of substrate solution. Selegiline (sigma; cat. no. S0360000) was used as the standard drug to inhibit the MAO-B enzyme. We used different sample concentrations ranging from 100 nm to 100 µM. The experiment was performed in triplicate to derive the mean error. Excitation and emission were measured at 545 nm and 590 nm, respectively.

$$\% \in Inhibition = \frac{[(Positivecontrol - Blanknegativecontrol) - (Sample - Samplecontrol)]}{(PositiveBlank - Blanknegativecontrol)} * 100\% \quad (1)$$

We used different concentrations of the sample/standard solution to evaluate the IC_{50} values using Equation (1).

3. Results and Discussion

3.1. Binding Site Analysis

Many PDB entries of MAO-B have been found to indicate the binding site of the particular protein. From these, high-resolution [1,6] crystal structures of MAO-B with PDB-id 2XFN, 2XCG, and 2XFU were used for binding site analysis using SiteMap. The most prominent binding site identified was a deep-seated cavity found in the MAO-B protein. Detailed analysis of the binding pocket showed that the binding site consisted of a hydrophilic site with an area of 6092, an acceptor site with an area of 2562, a donor site with an area of 3452, and a hydrophobic site with an area of 1452 (Figure 2). The PDB entry 2XCG and 2V60 were used as a template structure to decipher the conformation of the ligand for binding to its template. Structural studies of the ligand with its MAO-B receptor were performed using Chimera version 1.16. These studies indicate that residues, namely Y60, F103, P104, W119, L164, L167, F168, L171, C172, I199, Q206, I316, Y326, F343, Y398, and sY435, were found to be involved in the interaction with bound ligands (Figure 3A). Previous studies have indicated that this deep-seated allosteric site can block the enzyme specifically and is dependent on the inhibitor size [61].

To determine the stability of the protein-ligand system in the solvated system, we subjected the system to molecular dynamics studies. Gromac's version 20.0.7 was used for MD studies for an extended 200 ns. The system was stable, indicating a low RMSD for 1 Armstrong (Figure 3B). The ligand and the protein receptor were stable, indicating little conformational variation. The MD studies showed that the binding site of both the protein and the ligand conformation could be used for further computational studies, including docking and pharmacological modeling.

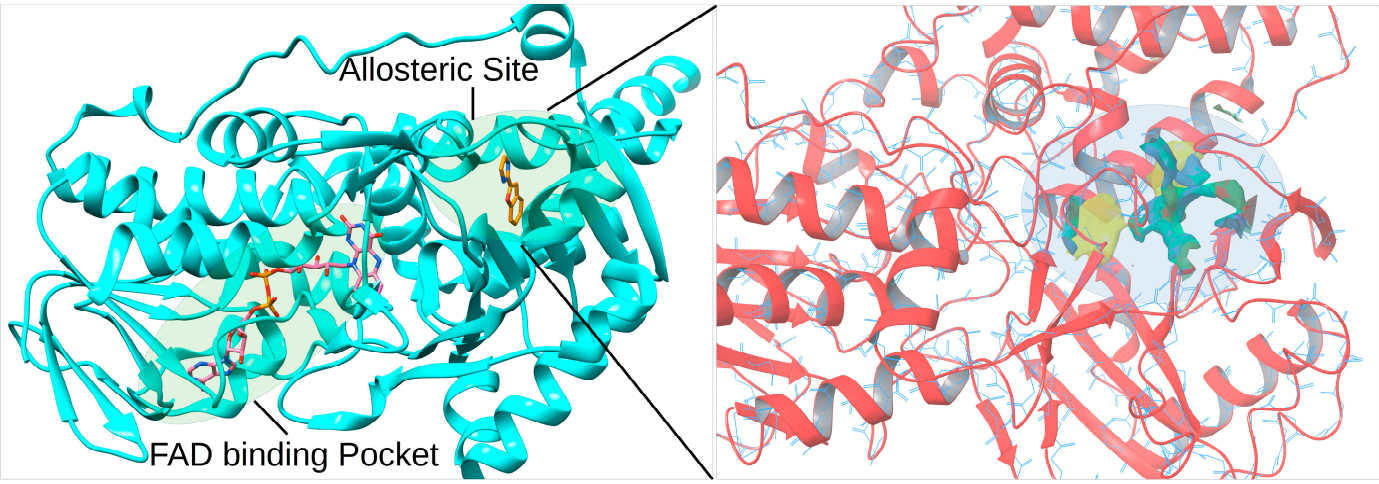

Figure 2. Indicates the full overlapped image of the acceptor (red), donor (blue), hydrophilic (green), and hydrophobic (yellow) region, respectively, in the binding site identified with the SiteMap module.

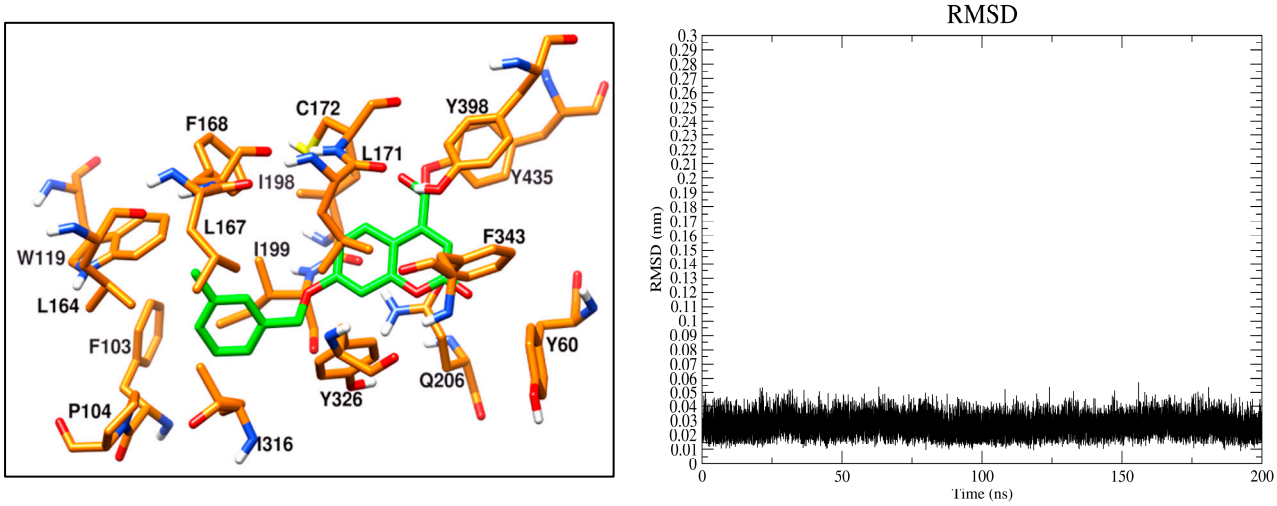

(**A**) (**B**)

Figure 3. (**A**) Indicates the residues involved in the interaction with the ligand. (**B**) Indicates the RMSD plot of the ligand.

3.2. Pharmacophore-Based Approach

Using the knowledge of the binding of ligands to protein pockets, 3 pharmacophore models were constructed. After the superposition of the ligands used for pharmacophore development, a pharmacophore hypothesis was generated using the ligands. Due to the enormous size of the ligands, numerous pharmacophore spots were generated in each of the four sets. The following criteria were used in the pharmacophore selection process: (1) The presence of donor, acceptor, and hydrophobic groups, as demonstrated by studies of the binding sites of the ligands to their receptors; (2) The propensity of the pharmacophore to recognize both active and inactive ligands. With two or more H-bonding acceptors and one or more hydrophobic and/or aromatic ring features, models could be representative, explaining the interactions for the most common fragments of known antagonists. All 6 pharmacophore models derived using the PHASE program were used to screen the ZINC database. The virtual screening was performed using a flexible search method. In reviewing the ligand-bound crystal structure of MaOB with inhibitors, 4-feature model 1 was used to further screen the ZINC database. The best pharmacophore generated had 2 hydrophobic groups (Hy1 and Hy2) and 2 acceptor sites (AA1 and AA2). Distance constraints had values of 9.70 +/− 0.90 between AA1 and Hy1 (D1), 6.44 +/− 0.60 between

Hy1 and Hy2, 4.89 +/− 0.40 between Hy2 and AA2, 5.94 +/− 0.50 between AA2 and AA1. The radii of the acceptor groups were 0.9, while they were 1 for the hydrophobic groups (Figure 4). Previous reports have used 3-feature pharmacophores for virtual screening, which generally yields a large number of hits and generally lacks specificity [62]. In comparison, our model has 4-features, which generally gives the model more specificity. A total of 875,776 hits were retrieved from the ZINC database using this pharmacophoric model. These hits were further subjected to an ML-based approach to further shortlist the hit molecules that display both fingerprinting and pharmacophoric features consistent with the already known inhibitors, and 20 poses were generated for each ligand identified using VS. These positions were then further examined visually to find potent inhibitors with a higher glide score than the established inhibitor selegiline.

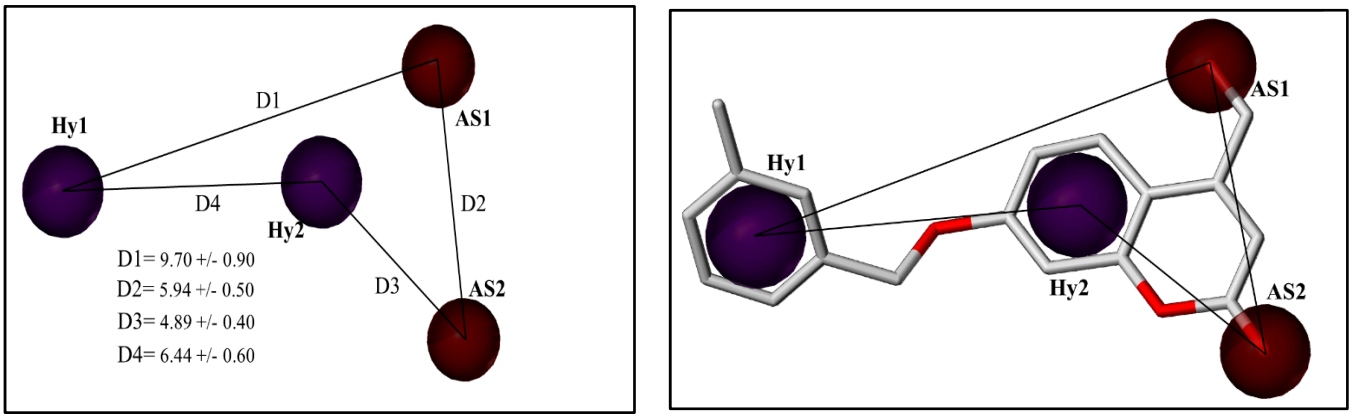

Figure 4. The image shows the pharmacological models generated with the PHASE module. This model yielded 875776 hits from the ZINC database after virtual screening.

3.3. ML-Based Screening

The activity data for the compounds against MAO B were downloaded from the CHEMBL database with ID CHEMBL2039. The dataset was verified as redundant. The range of activity of molecules in the data set from 0.014 nM to 58.9 mM gives us a wide range of inhibitors with different activities. Compounds with IC50 values less than 1M were treated as active molecules, while those with IC50 values greater than 1M were treated as inactive. So, using the above criteria, we had 2084 confirmed active and 3009 confirmed inactive molecules. The entire data set is divided into 75% training and 25% test sets. These binary ratios were used in the previous manuscript [63]. So there were 3820 connections in the training set and 1273 connections in the test set, as shown in Table 1. The active ingredients in the data set were marked with 1, while the inactive ones were marked with 0.

Table 1. Training and test datasets used in our study.

Dataset	Inhibitor	Non-Inhibitor	Total
Training	1563	2257	3820
Test	521	752	1273

For this dataset, we created 2071 descriptors using the PaDEL program. We selected the descriptors with a higher correlation coefficient to activity using the greedy technique. There were 186 descriptors in the reduced data set with a high correlation coefficient to activity. The ML models were constructed using several techniques using the descriptor data set. ML models were built using Python 3.6's scikit-learn module. We created six models commonly used to solve binary classification problems using descriptor data. The training and testing accuracy for the LR model were 0.895 and 0.805, respectively, while the area under the curve (AUC) of the ROC curve was 0.870. For the LR model, the precision

and recall values were 0.81 and 0.81, respectively. We achieved a training and testing accuracy for the decision tree model of 0.860 and 0.787, respectively, while the AUC of the ROC curve was 0.780. For the decision tree model, the precision and recall values were 0.81 and 0.81, respectively. We achieved a training and testing accuracy for the HR model of 0.974 and 0.821, respectively, and an AUC of the ROC curve of 0.888. For the RF model, the precision and recall values were 0.82 and 0.82, respectively. The training and testing accuracy for the SVM model was 0.955 and 0.818, respectively, and the AUC of the ROC curve was 0.850. The precision and recall values of the SVM model were 0.82 and 0.82, respectively. We were able to achieve a training and testing accuracy for the decision tree model of 0.860 and 0.787, respectively, while the AUC of the ROC curve was 0.780. For the decision tree model, the precision and recall values were 0.81 and 0.81, respectively. We were able to achieve training and testing accuracy for the HR model of 0.974 and 0.821, respectively, and an AUC of the ROC curve of 0.888. For the RF model, the precision and recall values were 0.82 and 0.82, respectively. The training and testing accuracy for the SVM model was 0.955 and 0.818, respectively, and the AUC of the ROC curve was 0.850. The precision and recall values of the SVM model were 0.82 and 0.82, respectively. The training and testing accuracy for the decision tree model was 0.860 and 0.787, respectively, while the area under the ROC curve (AUC) was 0.780. The precision and recall scores of the decision tree model were 0.81 and 0.81, respectively. The training and testing accuracy for the HF model was 0.974 and 0.821, respectively, and the AUC of the ROC curve was 0.888. The precision and recall values of the RF model were 0.82 and 0.82, respectively. We were able to achieve training and testing accuracy for the SVM model of 0.955 and 0.818, respectively, with a ROC curve AUC of 0.850. The precision and recall values of the SVM model were 0.82 and 0.82, respectively. We were able to achieve training and testing accuracy for the MLP model of 0.964 and 0.829, respectively, with a ROC curve AUC of 0.894. For the MLP model, the precision and recall values were 0.83 and 0.83, respectively. The training and testing accuracy for the XGB model was 0.967 and 0.846, respectively, and the AUC of the ROC curve was 0.916. For the XGB model, the precision and recall values were 0.86 and 0.85, respectively. We found that the XG-Boost model had the largest values for the statistical parameters, followed by the MLP model after all the statistical values of the different models were compared (Figure 5). Compared to the previous ML models used to screen MAO-B inhibitors, our model had higher statistical accuracy [64]. Table 2 summarizes the statistics of all models. Based on these values, the MLP model was used to screen the HDB1 database using the ML approach.

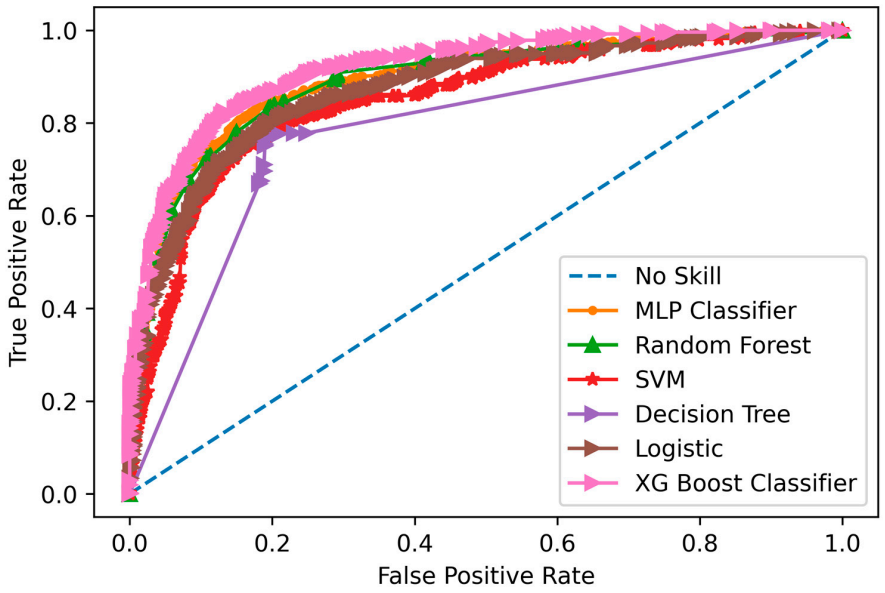

Figure 5. Image 3A indicates the AUC curve of different ML models generated using scikit-learn. The XG model indicated in pink had the highest area in the ROC curve.

Table 2. The table indicates the statistical value of different ML models.

Name of Model	Logistic Regression	Decision Tree	Random Forest	Support Vector Machine	Multilayer Perceptron	XG-Boost
Training Accuracy	0.895	0.860	0.974	0.955	0.964	0.967
Test Accuracy	0.805	0.787	0.821	0.818	0.829	0.846
Area Under Curve	0.870	0.780	0.888	0.850	0.894	0.916
Precision	0.81	0.79	0.82	0.82	0.83	0.86
Recall	0.81	0.79	0.82	0.82	0.83	0.85

Potential hit compounds against MAO B were found using the 875,776 molecule HDB1 database. All descriptors were originally generated with the PaDEL program and recorded in .csv format. Pandas was used to load the descriptor file as a data frame. From the HDB1 descriptor file, the relevant descriptors were selected and used to construct ML models for the MAO-B receptor. After separating the descriptors, a new data frame was created, and the MLP model was used for screening. From the HDB1 database, we could locate 66,784 molecular fingerprint hits that matched those of the drugs. We have created a new database of these 66,784 hits, namely HDB2.

3.4. Shape Screening-Based Approach

To further filter out shape-complementary hits with the known ligands, we used a shape-screening-based approach (Figure 6). Using the shape-based screening approach, we also sorted out 3978 hits from the HDB2 database of 66,784 entries. These hits were saved as a new database file HDB3. The database was further screened out based on binding affinity to the receptor using the docking-based approach.

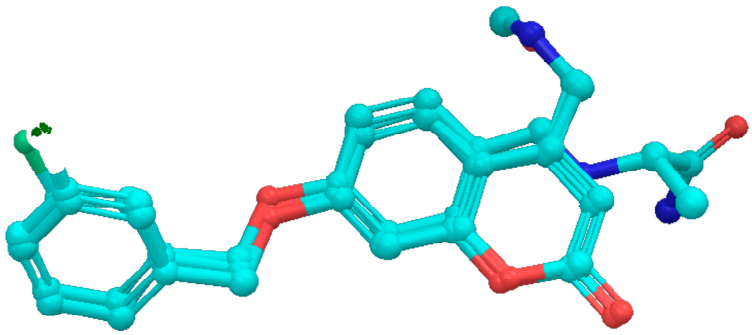

Figure 6. Multi-template conformation of ligand used for shape screening module of Schrodinger-2022-1.

3.5. Docking-Based Approach

The hits screened after shape screening were further evaluated for their binding affinity to protein using a docking-based approach. The generated Glide receptor lattice was used to dock ligands using the XP module, and top hits were identified with a higher GScore than the reported active control compound. The re-docking studies showed a low RMSD of 0.14 Armstrong (Figure 7). All information was compared to a grid constructed on the active site of the MAO-B enzyme using the Schrodinger glide module. The Schrödinger package's SiteMap module was used to create the binding pocket. Additionally, the grid generation module of the Schrödinger software package was used to generate the grid surrounding the protein. The protein and ligand preparation module of the Schrodinger software suite was used to prepare both the protein and the ligands. The Glide module was then used to dock the finished ligands. Docking was performed in Extra Precision mode on hits identified through shape screening, and parameters optimized during re-docking studies were used for docking. Chimera-1.16 and the ligand-receptor interaction module of the Schrödinger software suite were used to create the images. These interactions, hydrogen

bonding, pi-pi interaction, pi-cation interaction, and salt bridges at a cutoff radius of 4 Å were studied in this module, and 20 poses were created for each ligand.

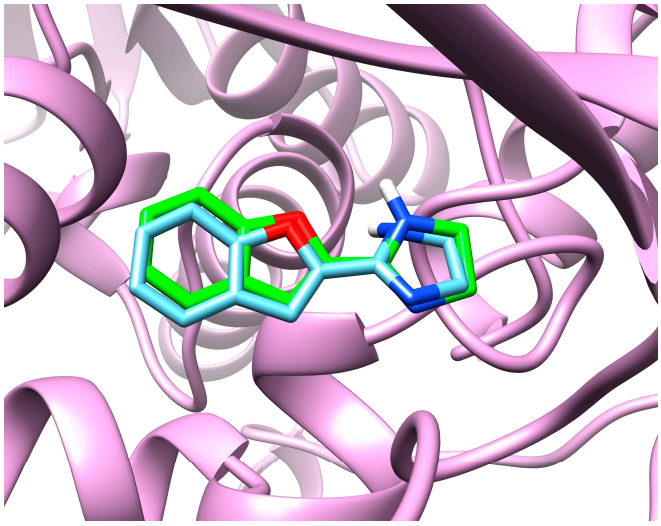

Figure 7. The image indicates the re-docked pose of the control molecule using Glide XP docking (cyan—co-crystallized pose, green—re-docked pose).

3.6. Identification of Top Hits

Using the primarily ML, pharmacophore, and docking-based approaches, we identified 54 hits with higher binding affinity than the selegiline compound. Docked reference poses from Glide Docking were used for further investigation (Figure 7), and 34 hits showing higher binding affinities than the control ligand for all three docking methods were filtered out by eye assessment. From these top 10 hits, further analysis was performed for their stability over time using MD studies.

3.7. MD Studies

In the current study, we performed a 200 ns run of molecular dynamics simulation for each hit ligand. After the molecular dynamics simulation run was completed, the resulting interaction patterns were studied. For each system, the backbone RMSD was determined and presented (Figure 8a,b).

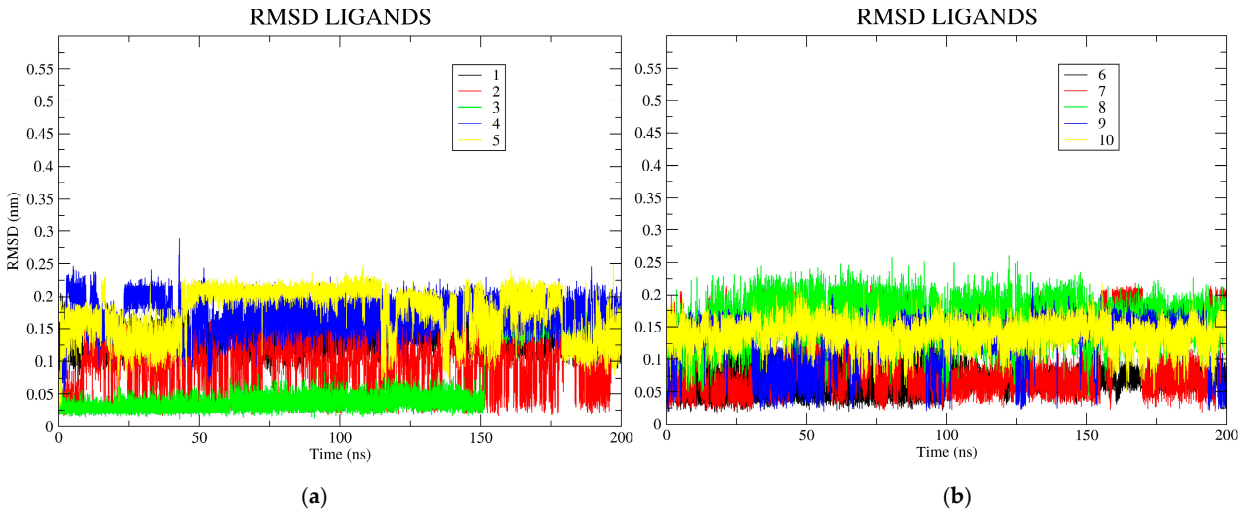

(**a**) (**b**)

Figure 8. (**a**,**b**) Indicates the RMSD plots of ligands. They were found to be highly stable. A low fluctuation of 2 Å was observed in RMSD ligand plots. These observations indicate the stability of the hits in the pocket of the receptor.

It was observed that 9 ligands from the ZINC database identified using different screening methods produced stable plots relative to RMSD plots generated using MD studies generated using Gromacs version 20.0.7 were carried out. Compared to some of the previously reported hit molecules using virtual screening, our best-selected molecules showed stable RMSD plots [64,65]. These compounds all showed deviations below 2 Å, indicating they are stable within the allosteric binding pocket in an extended MD run of 200 ns (Table 3).

Table 3. Summary of docking scores from various docking packages obtained for ligands identified for enzyme-based screening. QikProp score for various ligands and TOPKAT mutagenicity prediction for ligands identified for enzyme-based screening.

Sr. No	Name of Compound	Code Used	Glide-XP Score	MM/PBSA	QLogPo/w	QLogBB	Mutagenicity
1.	ZINC1028120	1	−10.917	−29.870	4.244	−0.184	Non-mutagenic
2.	KM00699	2	−10.858	−27.088	4.479	0.312	Non-mutagenic
3.	ZINC4523822	3	−10.614	−27.841	2.836	−0.937	Non-mutagenic
4.	BTB11789	4	−10.223	−10.391	5.404	0.312	Non-mutagenic
5.	ZINC171676	5	−10.130	−26.405	5.409	0.037	Non-mutagenic
6.	ZINC52610	6	−9.629	−28.487	5.404	−0.048	Non-mutagenic
7.	ZINC120336	7	−9.45	−27.406	5.357	0.212	Non-mutagenic
8.	HAN000359	8	−9.259	−20.451	3.134	−0.184	Non-mutagenic
9.	ZINC131390868	9	−9.113	−10.391	5.404	0.312	Non-mutagenic
10.	ZINC122521	10	−9.092	−25.666	4.747	0.485	Non-mutagenic
11.	SELEGILINE	Control	−9.102	−23.017	3.192	0.636	Non-mutagenic

3.8. Molecular Interaction Studies

By comparing the residues involved in the protein–ligand contact before and after the MD run, the molecular interactions of the stabilized complexes were investigated. For compound **1**, the residues involved in the interaction were Ile199, Tyr398, Tyr326, Phe343, Ile316, Leu164, Pro104, Trp119, Phe168, Cys172, Leu171, and Leu167. For compound **2**, the residues involved in the interaction were Gln206, Ile199, Tyr398, Phe343, Tyr326, Ile316, Leu164, Pro104, Trp119, Phe168, Cys172, and Leu171. For compound **3**, the residues involved in the interaction were Gln206, Ile199, Ile198, Tyr398, Tyr326, Phe343, Ile316, Leu164, Pro104, Trp119, Phe168, Cys172, and Leu171. For compound **4**, the residues involved in the interaction were Ile199, Ile198, Tyr398, Tyr435, Tyr326, Phe343, Ile316, Phe103, Pro104, Trp119, Phe168, Cys172, and Leu171 (Figure 9a,j).

For compound **5**, the residues involved in the interaction were Tyr435, Phe343, Gly205, Gln206, Gln65, Tyr60, Gly58, Tyr398, Ile198, Cys172, and Leu171. For compound **6**, residues Tyr435, Gln206, Ile199, Ile198, Tyr188, Leu164, Leu171, Trp119, Phe168, Cys172, and Leu171 were involved in the interaction. Namely, in compound **7**, residues Gln206, Ile199, Tyr398, Tyr435, Tyr326, Leu164, Trp119, Phe168, Cys172, and Leu171 were involved in the interaction.

From a careful analysis of the ligands with the protein MaO-B, we deduced that the hydrophobic binding groove formed by residues Phe103, Pro104, Leu164, Leu167, Phe168, Ile316, Leu171, Ile198 incidentally plays an important role in the binding of hit molecules plays other residues in close proximity (Figure 10a).

Residues, namely Tyr398, Tyr326, and Cys172, may also play a role in pi-cation and hydrogen-bonding interactions, preserving the antagonists in the binding groove (Figure 10b).

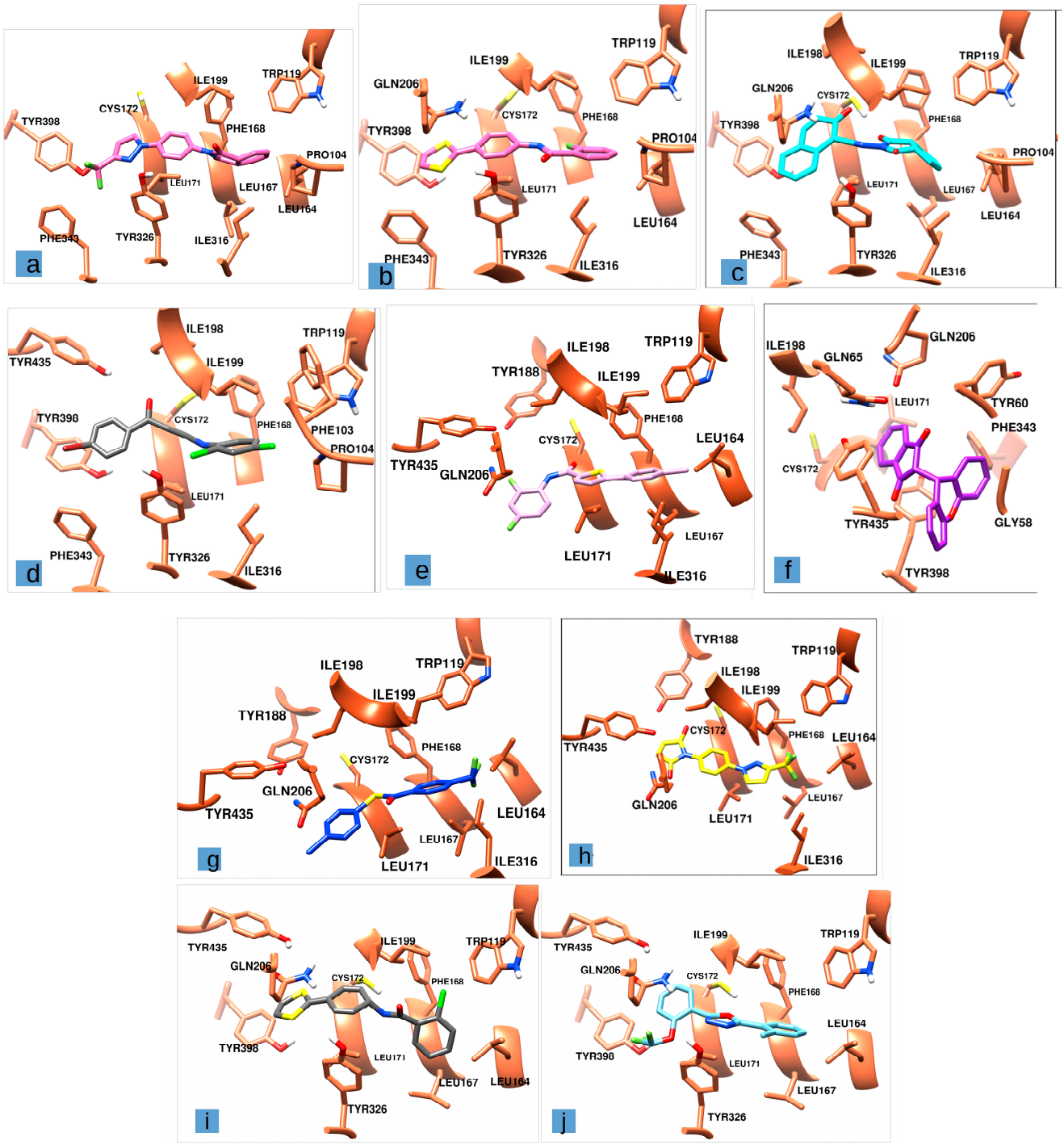

Figure 9. Panels image (**a**–**j**) show the residues involved in interactions with compounds **1**–**10**, respectively.

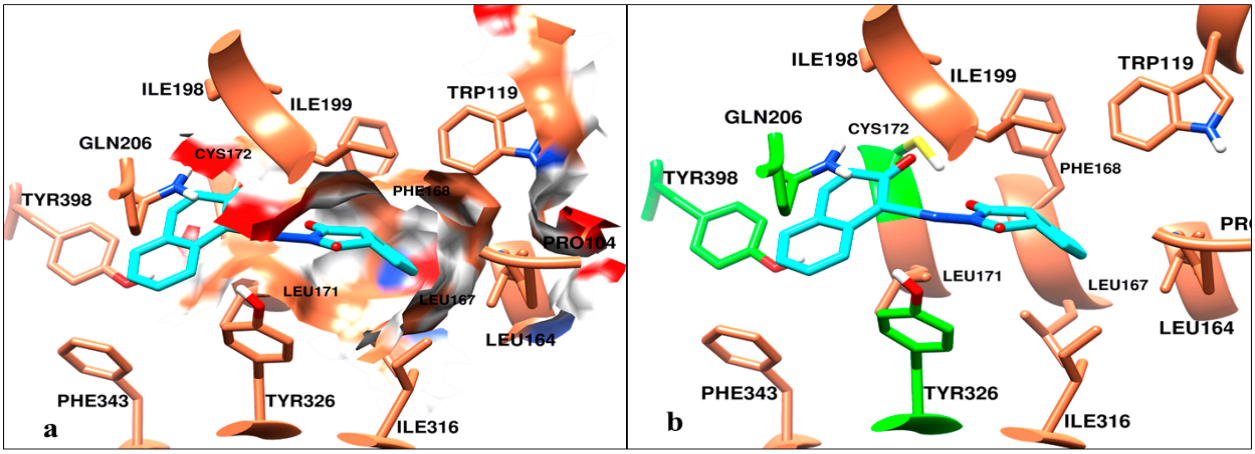

Figure 10. Image (**a**) shows the residues that form a hydrophobic pocket in MaO-B and are critical for the interaction with the ligands. (**b**) shows the residues (green) involved in hydrogen bonding and pi-cation interactions.

3.9. MAO Inhibition

Six different concentrations of sample/standard solution were tested to calculate IC_{50} values via enzyme assay activity. Briefly, the sample solution was pre-incubated with 2.5-µg MAO-B enzyme for 30 min at 37 °C. The reaction was initiated by adding 200 µM Amplex Red, 1 µM benzylamine (substrate for MAO-B enzyme), and 1 U/mL HRP. After performing the enzyme-based assay, we observed that compounds, namely **1** and **3**, showed excellent enzyme inhibitory activity of 0.37 µM and 0.55 µM, respectively. Moreover, it was also observed that the other three compounds, namely **2**, **5**, and **6**, showed an enzyme inhibitory activity of 3.67 µM, 13.6 µM, and 6.82 µM, respectively. In summary, we identified 5 molecules with inhibitory activity against MAO-B protein. The inhibitory activity of compounds has been tabulated in Table 4.

Table 4. IC_{50} values of MAO-B inhibitors.

Compounds	IC_{50}
1	0.36 ± 0.02 µM
2	3.67 ± 0.06 µM
3	0.54 ± 0.06 µM
5	13.2 ± 0.15 µM
6	6.82 ± 0.14 µM
Control	0.06 ± 0.01 µM

4. Conclusions

In this study, we presented a reliable computational model for the rational design and identification of MAO-B protein inhibitors. Using the large set of protein-ligand crystal structures, we were able to characterize the receptor's binding site, which has a deep-seated allosteric cavity that plays an important role in compound binding. Previously, the site has been used for targeting MAO-B protein. Various coumarin, isoxazole, and xanthone-based derivatives have been developed as novel inhibitors for targeting MAO-B. The binding site consists of a single large hydrophobic site along with small isolated patches of acceptors, donors, and hydrophilic sites. We could exclude 54 inhibitor compounds with higher binding energies than selegiline, a previously known drug, using binding site knowledge. The stability of these top 12 molecules was rigorously examined over time to identify the top molecules, which were selected for enzyme-based screening. A further six molecules had a fairly stable conformation with respect to the MaO-B protein. The interaction pattern

of the hit molecules at the molecular level after the MD simulation run suggests that the hydrophobic protein pocket formed by residues Phe103, Pro104, Leu164, Leu167, Leu171, Ile198, Ile199, Phe168, and Ile31, and nearby hydrophobic residues is a crucial one play a role in ligand binding. In addition, it was shown that residues Cys172, Tyr326, and Tyr398 are in the ideal orientation to play a significant role in contact. These residues can serve as pi-electron-sharing groups, donor groups, or both, completing the oppositely positioned acceptor groups in ligands. The top 5 inhibitors were subjected to an enzyme-based analysis to further support our theory. We identified 2 new inhibitors, 1 and 3, with IC_{50} values of 0.37 and 0.55 in the sub-micromolar range, respectively. In addition, molecules 2 and 6 were found to have an affinity of 3.67 and 6.82 μM, respectively. These four molecules can be further optimized to increase potency against MAO-B protein. Further MD trajectory analysis was performed on the ligand bound to the receptor protein to find the reasons for the differential activity of the ligand in an enzyme-based assay. However, we recognize that our studies lack in vivo studies of the best-identified molecules. In our future endeavor, the focus will be on in vivo studies of the top molecules to determine the pharmacokinetic and pharmacodynamic parameters. Our studies can be used to identify new and specific MAO-B inhibitors from other chemical databases. The approach can also be applied to screen hit molecules for other protein targets for other diseases.

Supplementary Materials: The following supporting information can be downloaded at: https://www.mdpi.com/article/10.3390/math11061464/s1. Figure S1: The flowchart indicates the role of the MAO-B enzyme in degrading the Dopamine hormone. Table S1: Table indicating the PDB entries of MAO-B inhibitors reported in the RCSB database.

Author Contributions: Conceptualization, A.J.S. and M.A.; methodology, S.J., A.K., M.A.S., M.M.A. and R.B.; validation, M.A., A.J.S., A.K., M.A.S., M.M.A. and S.J.; formal analysis, R.B. and M.A.; investigation, A.J.S., R.B., A.K., M.A.S., M.M.A. and S.J.; data curation, M.A., M.A.S., A.K., M.M.A. and R.B.; writing—original draft preparation, A.J.S. and M.A.; writing—review and editing, A.J.S., M.A.S. and S.J.; visualization, M.A.S. and R.B.; supervision, A.J.S. and M.A.; project administration, A.J.S. All authors have read and agreed to the published version of the manuscript.

Funding: This research has been funded by King Salman Center for Disability Research through Research Group No. KSRG-2022-086.

Data Availability Statement: Not applicable.

Acknowledgments: The authors thank the King Salman Center for Disability Research for funding this work through Research Group No. KSRG-2022-086.

Conflicts of Interest: The authors declare they have no competing financial interests.

References

1. Herraiz, T.; González, D.; Ancín-Azpilicueta, C.; Arán, V.J.; Guillén, H. beta-Carboline alkaloids in Peganum harmala and inhibition of human monoamine oxidase (MAO). *Food Chem. Toxicol. Int. J. Publ. Br. Ind. Biol. Res. Assoc.* **2010**, *48*, 839–845. [CrossRef]
2. Duncan, J.; Johnson, S.; Ou, X.M. Monoamine oxidases in major depressive disorder and alcoholism. *Drug Discov. Ther.* **2012**, *6*, 112–122. [CrossRef]
3. Shih, J.C.; Chen, K.; Ridd, M.J. Monoamine oxidase: From genes to behavior. *Annu. Rev. Neurosci.* **1999**, *22*, 197–217. [CrossRef] [PubMed]
4. Bortolato, M.; Chen, K.; Shih, J.C. Monoamine oxidase inactivation: From pathophysiology to therapeutics. *Adv. Drug Deliv. Rev.* **2008**, *60*, 1527–1533. [CrossRef] [PubMed]
5. Chen, J.J.; Swope, D.M. Pharmacotherapy for Parkinson's disease. *Pharmacotherapy* **2007**, *27*, 161s–173s. [CrossRef] [PubMed]
6. Riederer, P.; Danielczyk, W.; Grünblatt, E. Monoamine oxidase-B inhibition in Alzheimer's disease. *Neurotoxicology* **2004**, *25*, 271–277. [CrossRef] [PubMed]
7. López-Muñoz, F.; Alamo, C.; Juckel, G.; Assion, H.J. Half a century of antidepressant drugs: On the clinical introduction of monoamine oxidase inhibitors, tricyclics, and tetracyclics. Part I: Monoamine oxidase inhibitors. *J. Clin. Psychopharmacol.* **2007**, *27*, 555–559. [CrossRef]
8. Riederer, P.; Laux, G. MAO-inhibitors in Parkinson's Disease. *Exp. Neurobiol.* **2011**, *20*, 1–17. [CrossRef]

9. Youdim, M.B.; Bakhle, Y.S. Monoamine oxidase: Isoforms and inhibitors in Parkinson's disease and depressive illness. *Br. J. Pharmacol.* **2006**, *147* (Suppl. S1), S287–S296. [CrossRef]
10. Stocchi, F.; Borgohain, R.; Onofrj, M.; Schapira, A.H.; Bhatt, M.; Lucini, V.; Giuliani, R.; Anand, R. A randomized, double-blind, placebo-controlled trial of safinamide as add-on therapy in early Parkinson's disease patients. *Mov. Disord. Off. J. Mov. Disord. Soc.* **2012**, *27*, 106–112. [CrossRef]
11. Youdim, M.B.; Bar Am, O.; Yogev-Falach, M.; Weinreb, O.; Maruyama, W.; Naoi, M.; Amit, T. Rasagiline: Neurodegeneration, neuroprotection, and mitochondrial permeability transition. *J. Neurosci. Res.* **2005**, *79*, 172–179. [CrossRef]
12. Finberg, J.P.; Gillman, K. Selective inhibitors of monoamine oxidase type B and the "cheese effect". *Int. Rev. Neurobiol.* **2011**, *100*, 169–190. [CrossRef]
13. Kare, P.; Bhat, J.; Sobhia, M.E. Structure-based design and analysis of MAO-B inhibitors for Parkinson's disease: Using in silico approaches. *Mol. Divers.* **2013**, *17*, 111–122. [CrossRef] [PubMed]
14. Mladenović, M.; Patsilinakos, A.; Pirolli, A.; Sabatino, M.; Ragno, R. Understanding the Molecular Determinant of Reversible Human Monoamine Oxidase B Inhibitors Containing 2H-Chromen-2-One Core: Structure-Based and Ligand-Based Derived Three-Dimensional Quantitative Structure-Activity Relationships Predictive Models. *J. Chem. Inf. Model.* **2017**, *57*, 787–814. [CrossRef] [PubMed]
15. Pisani, L.; Farina, R.; Nicolotti, O.; Gadaleta, D.; Soto-Otero, R.; Catto, M.; Di Braccio, M.; Mendez-Alvarez, E.; Carotti, A. In silico design of novel 2H-chromen-2-one derivatives as potent and selective MAO-B inhibitors. *Eur. J. Med. Chem.* **2015**, *89*, 98–105. [CrossRef]
16. Ramesh, M.; Dokurugu, Y.M.; Thompson, M.D.; Soliman, M.E. Therapeutic, Molecular and Computational Aspects of Novel Monoamine Oxidase (MAO) Inhibitors. *Comb. Chem. High Throughput Screen* **2017**, *20*, 492–509. [CrossRef] [PubMed]
17. Agrawal, N.; Mishra, P. Synthesis, monoamine oxidase inhibitory activity and computational study of novel isoxazole derivatives as potential antiparkinson agents. *Comput. Biol. Chem.* **2019**, *79*, 63–72. [CrossRef]
18. Mubashir, N.; Fatima, R.; Naeem, S. Identification of Novel Phyto-chemicals from Ocimum basilicum for the Treatment of Parkinson's Disease using In Silico Approach. *Curr. Comput. Aided Drug. Des.* **2020**, *16*, 420–434. [CrossRef]
19. Schrödinger, L. *Schrödinger Suite*; Schrödinger, LLC: New York, NY, USA, 2016.
20. Bonivento, D.; Milczek, E.M.; McDonald, G.R.; Binda, C.; Holt, A.; Edmondson, D.E.; Mattevi, A. Potentiation of ligand binding through cooperative effects in monoamine oxidase B. *J. Biol. Chem.* **2010**, *285*, 36849–36856. [CrossRef]
21. Pettersen, E.F.; Goddard, T.D.; Huang, C.C.; Couch, G.S.; Greenblatt, D.M.; Meng, E.C.; Ferrin, T.E. UCSF Chimera–a visualization system for exploratory research and analysis. *J. Comput. Chem.* **2004**, *25*, 1605–1612. [CrossRef]
22. Páll, S.; Abraham, M.J.; Kutzner, C.; Hess, B.; Lindahl, E. Tackling exascale software challenges in molecular dynamics simulations with GROMACS. In Proceedings of the International Conference on Exascale Applications and Software, Stockholm, Sweden, 2–3 April 2014; pp. 3–27.
23. Binda, C.; Wang, J.; Pisani, L.; Caccia, C.; Carotti, A.; Salvati, P.; Edmondson, D.E.; Mattevi, A. Structures of human monoamine oxidase B complexes with selective noncovalent inhibitors: Safinamide and coumarin analogs. *J. Med. Chem.* **2007**, *50*, 5848–5852. [CrossRef] [PubMed]
24. Berman, H.M.; Westbrook, J.; Feng, Z.; Gilliland, G.; Bhat, T.N.; Weissig, H.; Shindyalov, I.N.; Bourne, P.E. The protein data bank. *Nucleic Acids Res.* **2000**, *28*, 235–242. [CrossRef]
25. Shivakumar, D.; Williams, J.; Wu, Y.; Damm, W.; Shelley, J.; Sherman, W. Prediction of Absolute Solvation Free Energies using Molecular Dynamics Free Energy Perturbation and the OPLS Force Field. *J. Chem. Theory Comput.* **2010**, *6*, 1509–1519. [CrossRef]
26. *Schrödinger Release 2017-3: LigPrep*; Schrödinger, LLC: New York, NY, USA, 2016.
27. Salam, N.K.; Nuti, R.; Sherman, W. Novel method for generating structure-based pharmacophores using energetic analysis. *J. Chem. Inf. Model.* **2009**, *49*, 2356–2368. [CrossRef]
28. *Schrödinger Release 2017-3: QikProp*; Schrödinger, LLC: New York, NY, USA, 2017.
29. Lipinski, C.A. Lead- and drug-like compounds: The rule-of-five revolution. *Drug Discov. Today Technol.* **2004**, *1*, 337–341. [CrossRef]
30. Leach, A. The ChEMBL database in 2017. *Nucleic Acids Res.* **2017**, *45*, D945–D954.
31. Yap, C.W. PaDEL-descriptor: An open source software to calculate molecular descriptors and fingerprints. *J. Comput. Chem.* **2011**, *32*, 1466–1474. [CrossRef] [PubMed]
32. Czub, N.; Pacławski, A. Do AutoML-Based QSAR Models Fulfill OECD Principles for Regulatory Assessment? A 5-HT(1A) Receptor Case. *Pharmaceutics* **2022**, *14*, 1415. [CrossRef]
33. Patel, L.; Shukla, T.; Huang, X.; Ussery, D.W. Machine Learning Methods in Drug Discovery. *Molecules* **2020**, *25*, 5277. [CrossRef]
34. Vamathevan, J.; Clark, D.; Czodrowski, P.; Dunham, I.; Ferran, E.; Lee, G.; Li, B.; Madabhushi, A.; Shah, P.; Spitzer, M. Applications of machine learning in drug discovery and development. *Nat. Rev. Drug Discov.* **2019**, *18*, 463–477. [CrossRef]
35. Pedregosa, F.; Varoquaux, G.; Gramfort, A.; Michel, V.; Thirion, B.; Grisel, O.; Blondel, M.; Prettenhofer, P.; Weiss, R.; Dubourg, V. Scikit-learn: Machine learning in Python. *J. Mach. Learn. Res.* **2011**, *12*, 2825–2830.
36. Khuri, N.; Deshmukh, S. Machine Learning for Classification of Inhibitors of Hepatic Drug Transporters. In Proceedings of the 2018 17th IEEE International Conference on Machine Learning and Applications (ICMLA), Orlando, FL, USA, 17–20 December 2018; pp. 181–186. [CrossRef]

37. Qu, J.; Wu, S.; Zhang, J. Flight Delay Propagation Prediction Based on Deep Learning. *Mathematics* **2023**, *11*, 494. [CrossRef]
38. Zhang, M.; Wang, Y.; Zhang, H.; Peng, Z.; Tang, J. A Novel and Robust Wind Speed Prediction Method Based on Spatial Features of Wind Farm Cluster. *Mathematics* **2023**, *11*, 499. [CrossRef]
39. Aboaoja, F.A.; Zainal, A.; Ali, A.M.; Ghaleb, F.A.; Alsolami, F.J.; Rassam, M.A. Dynamic Extraction of Initial Behavior for Evasive Malware Detection. *Mathematics* **2023**, *11*, 416. [CrossRef]
40. Li, Y.; Tian, Y.; Qin, Z.; Yan, A. Classification of HIV-1 Protease Inhibitors by Machine Learning Methods. *ACS Omega* **2018**, *3*, 15837–15849. [CrossRef]
41. Kawamura, Y.; Takasaki, S.; Mizokami, M. Using decision tree learning to predict the responsiveness of hepatitis C patients to drug treatment. *FEBS Open. Bio* **2012**, *2*, 98–102. [CrossRef]
42. Xia, Z.; Yan, A. Computational models for the classification of mPGES-1 inhibitors with fingerprint descriptors. *Mol. Divers.* **2017**, *21*, 661–675. [CrossRef]
43. Zhang, M.; Xia, Z.; Yan, A. Computer modeling in predicting the bioactivity of human 5-lipoxygenase inhibitors. *Mol. Divers.* **2017**, *21*, 235–246. [CrossRef]
44. Kalafi, E.Y.; Nor, N.A.M.; Taib, N.A.; Ganggayah, M.D.; Town, C.; Dhillon, S.K. Machine Learning and Deep Learning Approaches in Breast Cancer Survival Prediction Using Clinical Data. *Folia Biol.* **2019**, *65*, 212–220.
45. Saini, R.; Agarwal, S.M. EGFRisopred: A machine learning-based classification model for identifying isoform-specific inhibitors against EGFR and HER2. *Mol. Divers.* **2022**, *26*, 1531–1543. [CrossRef]
46. Cortes, C.; Vapnik, V. Support-vector networks. *Mach. Learn.* **1995**, *20*, 273–297. [CrossRef]
47. Mucherino, A.; Papajorgji, P.J.; Pardalos, P.M. K-nearest neighbor classification. In *Data Mining in Agriculture*; Springer: Berlin/Heidelberg, Germany, 2009; pp. 83–106.
48. Wu, X.; Kumar, V.; Ross Quinlan, J.; Ghosh, J.; Yang, Q.; Motoda, H.; McLachlan, G.J.; Ng, A.; Liu, B.; Yu, P.S. Top 10 algorithms in data mining. *Knowl. Inf. Syst.* **2008**, *14*, 1–37. [CrossRef]
49. Yu, H.-F.; Huang, F.-L.; Lin, C.-J. Dual coordinate descent methods for logistic regression and maximum entropy models. *Mach. Learn.* **2011**, *85*, 41–75. [CrossRef]
50. Pal, S.K.; Mitra, S. Multilayer perceptron, fuzzy sets, and classifiaction. *IEEE Trans. Neural Netw.* **1992**, *3*, 683–697. [CrossRef] [PubMed]
51. Ho, T.K. Random decision forests. In Proceedings of the 3rd International Conference on Document Analysis and Recognition, Montreal, QC, Canada, 14–16 August 1995; pp. 278–282.
52. Sastry, G.M.; Dixon, S.L.; Sherman, W. Rapid shape-based ligand alignment and virtual screening method based on atom/feature-pair similarities and volume overlap scoring. *J. Chem. Inf. Model.* **2011**, *51*, 2455–2466. [CrossRef]
53. *2022-3: S.R. MacroModel*; Schrödinger, LLC: New York, NY, USA, 2021.
54. Friesner, R.A.; Murphy, R.B.; Repasky, M.P.; Frye, L.L.; Greenwood, J.R.; Halgren, T.A.; Sanschagrin, P.C.; Mainz, D.T. Extra precision glide: Docking and scoring incorporating a model of hydrophobic enclosure for protein-ligand complexes. *J. Med. Chem.* **2006**, *49*, 6177–6196. [CrossRef] [PubMed]
55. Friesner, R.A.; Banks, J.L.; Murphy, R.B.; Halgren, T.A.; Klicic, J.J.; Mainz, D.T.; Repasky, M.P.; Knoll, E.H.; Shelley, M.; Perry, J.K.; et al. Glide: A new approach for rapid, accurate docking and scoring. 1. Method and assessment of docking accuracy. *J. Med. Chem.* **2004**, *47*, 1739–1749. [CrossRef] [PubMed]
56. Sharma, T.; Harioudh, M.K.; Kuldeep, J.; Kumar, S.; Banerjee, D.; Ghosh, J.K.; Siddiqi, M.I. Identification of Potential Inhibitors of Cathepsin-B using Shape & Pharmacophore-based Virtual Screening, Molecular Docking and Explicit Water Thermodynamics. *Mol. Inform.* **2020**, *39*, e1900023. [CrossRef]
57. Sharma, T.; Baig, M.H.; Khan, M.I.; Alotaibi, S.S.; Alorabi, M.; Dong, J.J. Computational screening of camostat and related compounds against human TMPRSS2: A potential treatment of COVID-19. *Saudi Pharm. J. SPJ Off. Publ. Saudi Pharm. Soc.* **2022**, *30*, 217–224. [CrossRef]
58. Sharma, T.; Siddiqi, M.I. In silico identification and design of potent peptide inhibitors against PDZ-3 domain of Postsynaptic Density Protein (PSD-95). *J. Biomol. Struct. Dyn.* **2019**, *37*, 1241–1253. [CrossRef]
59. Kalyane, D.; Sanap, G.; Paul, D.; Shenoy, S.; Anup, N.; Polaka, S.; Tambe, V.; Tekade, R.K. Artificial intelligence in the pharmaceutical sector: Current scene and future prospect. In *The Future of Pharmaceutical Product Development and Research*; Elsevier: Amsterdam, The Netherlands, 2020; pp. 73–107.
60. Sharma, T.; Saralamma, V.V.G.; Lee, D.C.; Imran, M.A.; Choi, J.; Baig, M.H.; Dong, J.-J. Combining structure-based pharmacophore modeling and machine learning for the identification of novel BTK inhibitors. *Int. J. Biol. Macromol.* **2022**, *222*, 239–250. [CrossRef] [PubMed]
61. Holt, A.; Berry, M.D.; Boulton, A.A. On the binding of monoamine oxidase inhibitors to some sites distinct from the MAO active site, and effects thereby elicited. *Neurotoxicology* **2004**, *25*, 251–266. [CrossRef] [PubMed]
62. Boppana, K.; Dubey, P.K.; Jagarlapudi, S.A.; Vadivelan, S.; Rambabu, G. Knowledge based identification of MAO-B selective inhibitors using pharmacophore and structure based virtual screening models. *Eur. J. Med. Chem.* **2009**, *44*, 3584–3590. [CrossRef]
63. Rodriguez-Perez, R.; Bajorath, J. Multitask machine learning for classifying highly and weakly potent kinase inhibitors. *ACS Omega* **2019**, *4*, 4367–4375. [CrossRef]

64. Dhanabalan, A.K.; Subaraja, M.; Palanichamy, K.; Velmurugan, D.; Gunasekaran, K. Identification of a Chlorogenic Ester as a Monoamine Oxidase (MAO-B) Inhibitor by Integrating "Traditional and Machine Learning" Virtual Screening and In Vitro as well as In Vivo Validation: A Lead against Neurodegenerative Disorders? *ACS Chem. Neurosci.* **2021**, *12*, 3690–3707. [CrossRef] [PubMed]
65. Olotu, F.A.; Joy, M.; Abdelgawad, M.A.; Narayanan, S.E.; Soliman, M.E.; Mathew, B. Revealing the role of fluorine pharmaco-phore in chalcone scaffold for shifting the MAO-B selectivity: Investigation of a detailed molecular dynamics and quan-tum chemical study. *J. Biomol. Struct. Dyn.* **2021**, *39*, 6126–6139. [CrossRef]